IAC-09-C1.5.4

ADVANCED MODELING OF OPTIMAL LOW-THRUST LUNAR POLE-SITTER TRAJECTORIES

Daniel J. Grebow
Ph.D. Candidate, School of Aeronautics and Astronautics
Purdue University, United States of America
grebow@purdue.edu

Martin T. Ozimek
Ph.D. Candidate, School of Aeronautics and Astronautics
Purdue University, United States of America
mozimek@purdue.edu

Kathleen C. Howell
Hsu Lo Professor, School of Aeronautics and Astronautics
Purdue University, United States of America
howell@purdue.edu

One immediate and cost-effective solution for lunar south pole coverage is a low-thrust pole-sitter spacecraft. When the spacecraft's fuel is nearly expended, it can also be used as part of a larger constellation that might require more time to deploy. This study examines the feasibility of the lunar pole-sitter from a dynamical standpoint. The model includes the effects of Earth oblateness, solar wind, gravity perturbations, and shadowing on a 500 kg spacecraft equipped with an NSTAR thruster. Lunar librations are also incorporated into path constraints on elevation angle and altitude from a potential ground station at the Shackleton crater. The solutions utilize multiple phases, including transfer-out from the International Space Station and spiral-down into a stable lunar orbit once the pole-sitting period is completed. Computation of the trajectory is based on a 12^{th}-order collocation scheme. A direct transcription routine maximizes the time in the coverage phase, increasing the time span from 387 to 451 days. During this period, the minimum elevation angle relative to the Shackleton crater site is 6°.

INTRODUCTION

Presently, NASA is exploring the moon, intending to establish a permanent human outpost by 2020. There is also great international interest in harvesting resources that might be available at or nearby the Shackleton crater near the lunar south pole, as evidenced by recent missions such as JAXA's Selenological and Engineering Explorer[1] (SELENE), NASA's Lunar Reconnaissance Orbiter[2] (LRO) and Lunar Crater Observation and Sensing Satellite[2] (LCROSS), and the Indian Space Research Organisation's Chandrayaan-1.[3] On September 24, 2009, confirmation of these potential resources was obtained by Chandrayaan-1, which used NASA's Moon Mineralogy Mapper (M3) to successfully detect water on the moon.[4] This recent discovery may motivate the selection of a human outpost location such as the Shackleton crater. This possible landing site continues to generate ongoing scientific interest, most recently by the Moon Impact Probe (MIP) of Chandrayaan-1, that targeted a region nearby Shackleton for signs of water ice. To support such a future manned south pole mission, there are many different trajectory options for the communications satellites.[5–7] One novel approach is a pole-sitter, as proposed by Grebow et al.[8] In the paper, the authors suggest the immediate deployment of a small 500 kg spacecraft from the International Space Station (ISS). Equipped with an NSTAR thruster, the spacecraft transfers to the vicinity of the moon and then maintains constant surveillance of the lunar south pole. After a significant surveillance period is completed, an added advantage of the mission is that the spacecraft uses its remaining fuel to spiral-down into a stable lunar orbit for continued surveillance; the spacecraft is then the first piece of a long duration, multiple-spacecraft constellation. Such a mission would be beneficial for temporarily maintaining constant surveillance with only one spacecraft, while waiting for the remaining spacecraft in the constellation, that are launched at a later time.

In the previous study,[8] optimal trajectories were successfully computed that satisfied the mission design objectives. However, only the Restricted Three-Body Problem (RTBP), with low-thrust acceleration, was used as a dynamical model. The dynamical effects of factors such as a higher-fidelity gravitational model and the space environment are important for gauging the true behavior and

corresponding performance of the spacecraft during a mission. For example, solar radiation pressure (SRP) is a significant perturbing force that is typically larger than the perturbing gravity force of the sun for Earth-moon applications. Previous research has indicated that SRP alone can shift the sun-Earth L_1 and L_2 libration points by over 100 kilometers.[9] Spacecraft with larger surface areas, such as a solar sail, can even exploit SRP to access non-Keplerian trajectories that continuously offset the spacecraft from a planet or moon's orbital plane.[10] The presence of the Earth's shadow also poses considerable complexity for a solar electric propulsion mission during the spiral-out from low-Earth orbit. As a result, the time-of-flight for a transfer sequence will increase, and is therefore frequently included in higher fidelity low-thrust simulations.[11,12] In particular, Flandro analytically demonstrates that a 27% time-of-flight penalty is incurred during his solar electric propulsion orbit-raising sequence when incorporating shadow entry and exit.[13] When implementing the eclipsing conditions due to shadowing, it is also essential to model the J_2 effects due to Earth oblateness. As noted by McInnes,[14] the nodal precession induced by oblateness over the course of long-duration spiraling will considerably affect the dynamical path. Finally, the effect of lunar librations alters the elevation angle performance during the evolution of pole-sitter orbits.[7]

The design of high-fidelity pole-sitter trajectories requires continuous path constraints. Additionally, sensitive dynamics, complicated system equations, and difficulties in acquiring an initial guess necessitate a wide convergence basin for any numerical algorithm that may be employed. Such problems are perhaps best solved using collocation.[15,16] In collocation schemes, path constraints for an entire phase are constantly enforced, and high sensitivity in a numerical search direction is best distributed over the entire trajectory. While a previous drawback to these approaches has been the large dimensionality, the current state of computing speed and the efficient handling of sparse linear systems has lessened the impact of these issues. In a study by Betts,[17] collocation was used to efficiently solve over 70 different trajectory optimization problems. For these reasons, the higher-order, Gauss-Lobatto collocation and direct transcription approaches detailed in Grebow et al.[8] are implemented for this study. Using this method, the multi-phase, pole-sitter trajectory is computed in the full model, including planetary ephemerides, lunar librations, SRP, Earth oblateness, and shadowing. The Earth-moon RTBP is the basic model for preliminary design of the pole-sitter trajectory, and serves as an initial guess for the high-fidelity solution. The feasible and optimal high fidelity trajectories are discussed and compared to the previous results.

PRELIMINARY DESIGN

Simplified Model

The design of a high-fidelity pole-sitter mission trajectory originates by considering the coverage phase in the Earth-moon Restricted Three-Body Problem (RTBP) with additional thrust $\boldsymbol{f}_T(t,\boldsymbol{u})$, where $\boldsymbol{u}$ is the control vector. In the Earth-moon RTBP, the Earth and moon are assumed to move in circular orbits, and the spacecraft possesses comparatively negligible mass. The standard rotating, barycentric coordinate frame is used, with the x-axis directed from the Earth to the moon and the z-axis parallel to the Earth-moon angular velocity. Using the traditional nondimensional form, the equations are written

$$\begin{aligned}\dot{\boldsymbol{x}} &= \boldsymbol{f}(t,\boldsymbol{x},\boldsymbol{u},\boldsymbol{\lambda}) = \begin{pmatrix}\dot{\boldsymbol{r}}\\ \dot{\boldsymbol{v}}\end{pmatrix}\\ &= \begin{Bmatrix}\boldsymbol{v}\\ \boldsymbol{f}_T(t,\boldsymbol{u}) - 2\boldsymbol{\Omega}\times\boldsymbol{v} + \nabla U(\boldsymbol{r})\end{Bmatrix}\end{aligned} \qquad [1]$$

where $\boldsymbol{\lambda}$ is a problem dependent parameter vector. Note that in Eqn. [1], x, y, and z are the components of the spacecraft's position relative to the rotating, barycentric frame. The mass parameter is μ, the Earth-moon angular velocity is $\boldsymbol{\Omega}$, and $\boldsymbol{r}_1$ and $\boldsymbol{r}_2$ are the positions of the Earth and moon, respectively. The equations are scaled by the total mass m^* of the system, the distance l^* between the Earth and moon, and characteristic time $t^* = (l^{*3}/Gm^*)^{1/2}$. When $\boldsymbol{f}_T(t,\boldsymbol{u}) = 0$, as occurs during a coasting arc, the motion is governed by the natural dynamics. The components within Eqn. [1] are derivable from the potential function

$$U = \frac{1-\mu}{\|\boldsymbol{r}-\boldsymbol{r}_1\|} + \frac{\mu}{\|\boldsymbol{r}-\boldsymbol{r}_2\|} + \frac{1}{2}\left(x^2+y^2\right) \qquad [2]$$

The RTBP dynamical model is useful during preliminary design to gain insight into the regions that a pole-sitter may occupy if $\dot{\boldsymbol{x}} = 0$ in Eqn. [1], i.e., if the spacecraft is to remain stationary with respect to the rotating frame. For $\dot{\boldsymbol{x}} = 0$, the thrust acceleration $\boldsymbol{f}_T$ must offset the gravity gradient term $\boldsymbol{\nabla} U$. For pole-sitter trajectories, a contour plot of $\|\boldsymbol{\nabla} U\|$ suffices to inspect approximate regions that are accessible to the spacecraft, given the limitations of the selected engine's thrust acceleration. (See Fig. 1.) In Fig. 1, it is clear that the RTBP is useful for basic modeling of a pole-sitter trajectory. Regions of low $\|\boldsymbol{\nabla} U\|$ extend from the libration points L_1 and L_2 (appearing as dark red dots on the x-axis). Given the limitations of current low-thrust acceleration devices, such as solar electric propulsion and solar sails, these regions are the only feasible locations for a pole-sitter orbit in the vicinity of the moon.

As a sample application using Fig. 1, consider a thrust acceleration value of $\|\boldsymbol{f}_T\| = 0.5$ mm/s^2. This numerical value is typical of a solar electric thruster, or possibly a very large solar sail. Inspection of the contours of constant $\|\boldsymbol{\nabla} U\|$ in Fig. 1 indicates that a pole-sitting spacecraft is, at least initially, restricted to the red regions. Larger thrust accelerations, those that might occur with a larger thruster or a smaller spacecraft mass, allow the satellite to potentially enter the yellow and green locations that wrap below the lunar south pole. Note that for solar electric engines, the coverage capabilities of the spacecraft will increase since $\|\boldsymbol{f}_T\|$ increases with fuel consumption when the thrust magnitude

and specific impulse are constant. Given the proper corrections algorithms to adjust the trajectory, this simple visual inspection approach for estimating the location of potential pole-sitting trajectories is a powerful tool that bypasses the need for more complicated numerical or analytical initial guess schemes.

Preliminary Results

Consistent with the previous study, the mission is separated into the following three phases:

1. Earth-centered, spiral-out to the Moon
2. Maintain the pole-sitting position for as long as possible
3. Moon-centered, spiral-down to an elliptically inclined stable orbit

The end-of-life orbit corresponds to a frozen orbit investigated by Ely,[5] and thus serves thereafter as part of a larger constellation for continued surveillance and lunar operations. The spacecraft is assumed to possess a wet mass of 500 kg and dry mass equal to 50 kg. It is equipped with an NSTAR thruster similar to Deep Space 1 (thrust 150 mN, specific impulse 1,650 s). The phases are initially designed independently, beginning with phase #2. Assuming that phases #1 and #3 require 180 kg and 2 kg of fuel, respectively, Fig. 1 is used to approximate an initial guess for the pole-sitter trajectory. The guess is separated into a specified number of thrusting and coasting arcs and a collocation routine locates a nearby solution satisfying Eqn. [1]. (See Grebow et al.[8] for details.) A sample feasible solution near L_2 with 36 thrust arcs appears in Fig. 2. Recall that the x-y plane corresponds to the moon orbit plane. Here, the orbit is positioned in a region approximately $38,400$ km below the L_2 point, and is within direct line-of-sight of the Shackleton Crater.

The trajectory appearing in Fig. 2 is precisely the trajectory that is to be transitioned to the full model. Once approximations for phases #1 and #3 are obtained in the full model, all three phases enter a larger collocation scheme that applies boundary conditions to ensure continuity between the phases. Since collocation problems are easily modified for optimization with direct transcription, the feasible solution serves as an initial guess for an optimal trajectory where SNOPT[18] optimizes the time interval associated with phase #2. The procedure has been successfully implemented in the RTBP, where the optimal trajectory extended the time for phase #2 from 447 days to 554 days.[8] For reference, an example of the feasible design from the previous study in the RTBP model in the rotating frame appears in Fig. 3. Here, the combination of phase #2 with the other phases is apparent, in addition to the stable lunar frozen orbit that serves as the end-of-life trajectory (in green).

ADVANCED MODELING

Several higher fidelity effects must be incorporated into a scheme to upgrade the accuracy. This investigation considers

1. Departure from an actual ISS state
2. Solar gravity perturbations
3. Relative positions of the sun, Earth, and moon from JPL DE405 ephemeris file
4. Earth oblateness
5. Solar radiation pressure
6. Shadowing for initial spiral-out from ISS
7. Path constraints to incorporate lunar librations
8. Lunar site shifted to longitude and latitude of the Shackleton crater

This section describes the inclusion of these effects in the dynamical model, and the development of the systematic procedure for computing low-thrust trajectories with coasting arcs.

System Equations

For the full model, the equations of motion in the moon-centered EMEJ2000 frame are written in a simplified form as

$$\begin{aligned} \dot{\boldsymbol{X}} &= \boldsymbol{f}(t,\boldsymbol{X},\boldsymbol{u},\boldsymbol{\lambda}) = \begin{pmatrix} \dot{\boldsymbol{R}} \\ \dot{\boldsymbol{V}} \end{pmatrix} \\ &= \begin{Bmatrix} \boldsymbol{V} \\ \boldsymbol{f}_M + \boldsymbol{f}_E + \boldsymbol{f}_S + \boldsymbol{f}_T \end{Bmatrix} \end{aligned} \quad [3]$$

where the vector $\boldsymbol{R}$ is the moon-centered EMEJ2000 position vector with components X, Y, and Z. As in Eqn. [1], the control is $\boldsymbol{u}$, and $\boldsymbol{\lambda}$ is a problem parameter vector. For all computations, Eqn. [3] is scaled with the same Earth-moon RTBP characteristic quantities, m^*, l^*, and t^*, as Eqn. [1]. The right-hand side of Eqn. [3] sums the acceleration vector $\boldsymbol{f}_M$ from lunar gravity, $\boldsymbol{f}_E$ from Earth gravity, $\boldsymbol{f}_S$ from solar gravity and radiation pressure, and the thrust force $\boldsymbol{f}_T$ from the solar electric spacecraft engine. The dominant acceleration, due to lunar gravity modeled as a point mass, is evaluated via the inverse square law

$$\boldsymbol{f}_M = -\mu_M \frac{\boldsymbol{R}}{\|\boldsymbol{R}\|^3} \quad [4]$$

The Earth accelerations are comprised of the perturbing terms

$$\begin{aligned} \boldsymbol{f}_E = & -\mu_E \left(\frac{\boldsymbol{R}_E}{\|\boldsymbol{R}_E\|^3} + \frac{\boldsymbol{R}-\boldsymbol{R}_E}{\|\boldsymbol{R}-\boldsymbol{R}_E\|^3} \right) \\ & -\frac{3}{2}\frac{\mu_E J_2 r_E^2}{\|\boldsymbol{R}-\boldsymbol{R}_E\|^5} \begin{Bmatrix} \alpha\left(1-5\dfrac{\gamma^2}{\|\boldsymbol{R}-\boldsymbol{R}_E\|^2}\right) \\ \beta\left(1-5\dfrac{\gamma^2}{\|\boldsymbol{R}-\boldsymbol{R}_E\|^2}\right) \\ \gamma\left(3-5\dfrac{\gamma^2}{\|\boldsymbol{R}-\boldsymbol{R}_E\|^2}\right) \end{Bmatrix} \end{aligned} \quad [5]$$

where $\boldsymbol{R}_E$ is the ephemeris position vector of the Earth relative to the moon and

$$\begin{aligned} \alpha &= X - X_E \\ \beta &= Y - Y_E \\ \gamma &= Z - Z_E \end{aligned} \quad [6]$$

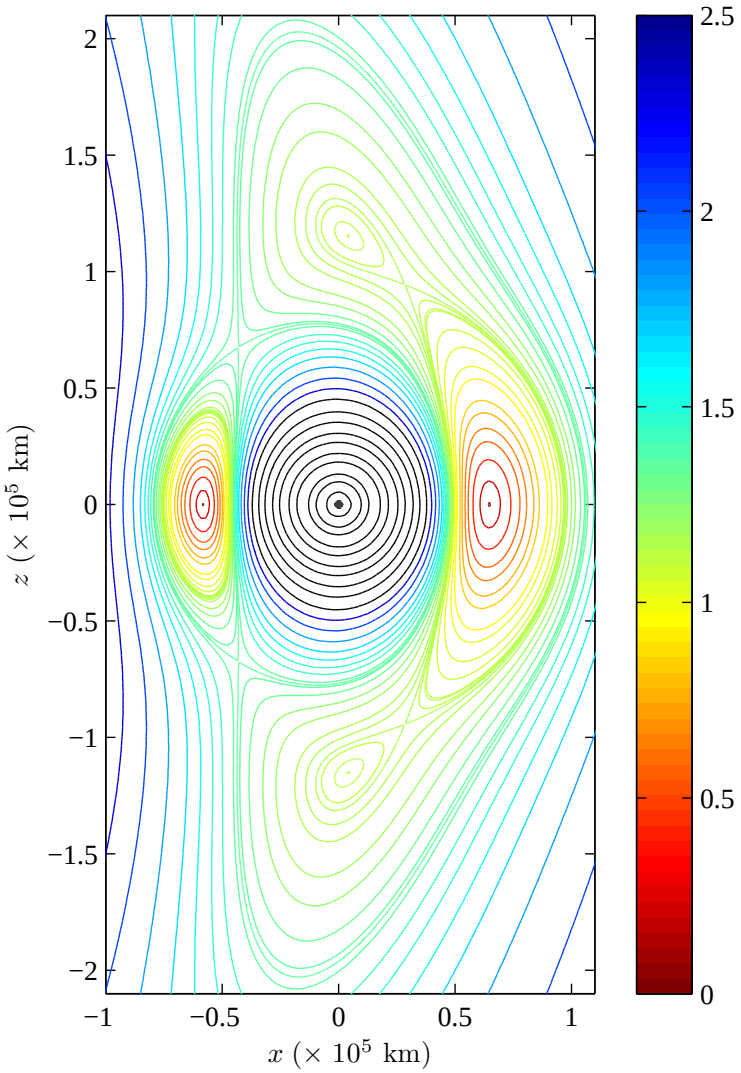

Fig. 1 Contours of $\|\nabla U\|$ in mm/s^2, Moon-Centered Rotating Frame.

The first term in Eqn. [5] is the perturbation due to the Earth's gravity when modeled as a point mass, and the second term incorporates the effect of Earth oblateness due to the J_2 term, where r_E is the mean radius of the Earth. The oblateness model assumes that the Earth's axis of rotation is fixed in inertial space along the positive Z-axis of the EMEJ2000 frame. The acceleration due to the sun, $\boldsymbol{f}_S$, is

$$\boldsymbol{f}_S = -\mu_S \left(\frac{\boldsymbol{R}_S}{\|\boldsymbol{R}_S\|^3} + \frac{\boldsymbol{R}-\boldsymbol{R}_S}{\|\boldsymbol{R}-\boldsymbol{R}_S\|^3} \right) - \frac{kAS_0 r_0^2}{cm} \frac{\boldsymbol{R}-\boldsymbol{R}_S}{\|\boldsymbol{R}-\boldsymbol{R}_S\|^3} \quad [7]$$

where $\boldsymbol{R}_S$ is the ephemeris position vector of the sun relative to the moon. Similar to Eqn. [5], the first term in Eqn. [7] is due to solar (point mass) gravity perturbations. The second term is the solar radiation pressure, where k is a material parameter dependent on absorptivity of the spacecraft surface, A is the projected cross-sectional area (a spherical body, and therefore a circular cross-section is assumed), c is the speed of light, S_0 is the solar light flux associated with the nominal distance $r_0 = 1$ AU, and m is the spacecraft mass. (For further detail, see Farquhar.[19]) Finally, the acceleration due to the solar electric thruster is modeled as

$$\boldsymbol{f}_T = \frac{T}{m_0 - t \cdot T/(g_0 I_{sp})} \frac{\boldsymbol{u}}{\|\boldsymbol{u}\|} \quad [8]$$

where T is the constant thrust magnitude, m_0 is the initial spacecraft mass, g_0 is the Earth gravitational acceleration constant at sea level, I_{sp} is the specific impulse, and $\boldsymbol{u}$ is the thrust direction control. (For numerical reasons, the spacecraft mass and thrust magnitude are scaled by m_0 instead of m^*.) This model assumes that sufficient power is always available for the engine to operate at a constant thrust level, even in the presence of array degradation. When the engine is off for coasting arcs, then $T = 0$ and therefore $\boldsymbol{f}_T = 0$.

Trajectory Computation

A general algorithm is developed to apply to each phase, with the exception that phase #2 incorporates path con-

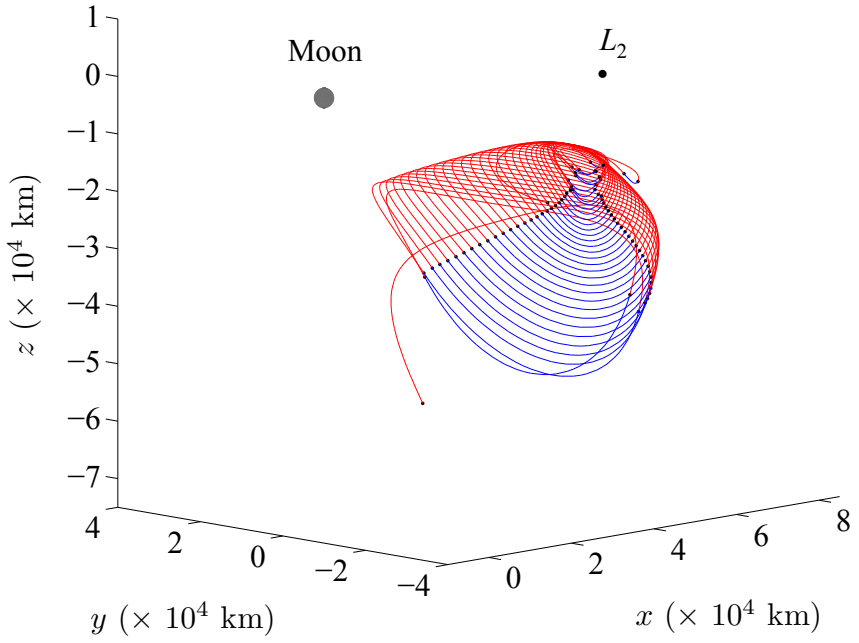

Fig. 2 Feasible Solution for Phase #2 in RTBP, Thrust Arcs (red) and Coast Arcs (blue).

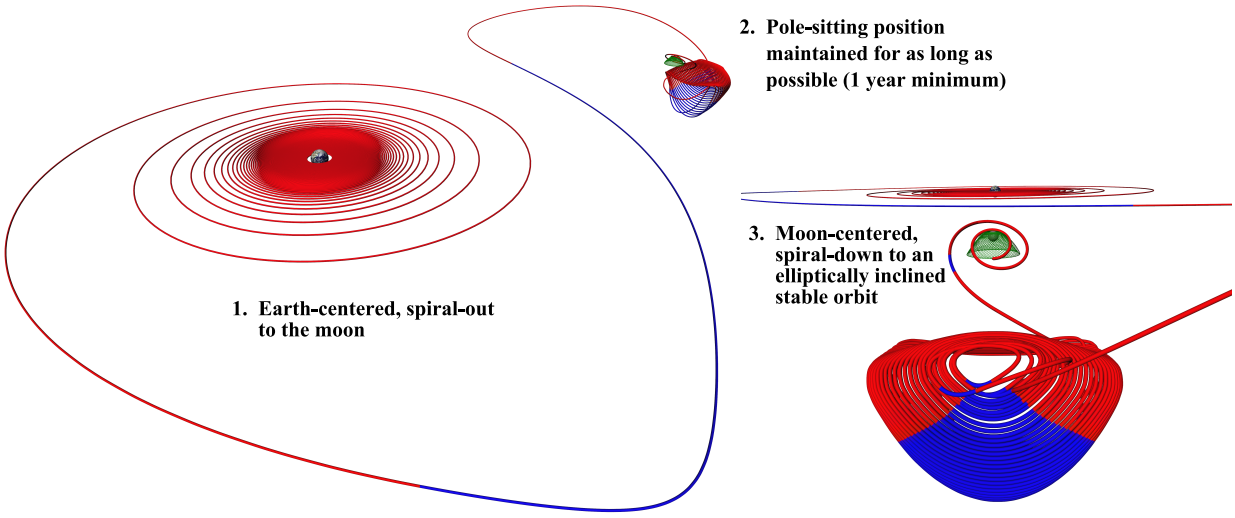

Fig. 3 Three-Phase Feasible Solution Previously Computed in the RTBP.[8]

strains on minimum elevation angle ϕ_{lb} and maximum altitude a_{ub} relative to the Shackleton site. Adapting the scheme in Ozimek et al.,[7] the continuous time path constraints that achieve this objective are

$$\boldsymbol{g}(\boldsymbol{R},\boldsymbol{\eta}) = \left\{ \begin{array}{c} \sin(\phi_{lb}) + \dfrac{\boldsymbol{R}_g \cdot (\boldsymbol{R}_g - \boldsymbol{R})}{||\boldsymbol{R}-\boldsymbol{R}_g||||\boldsymbol{R}_g||} \\ ||\boldsymbol{R}-\boldsymbol{R}_g|| - a_{ub} \end{array} \right\} + \boldsymbol{\eta}^2 = 0 \quad [9]$$

where $\boldsymbol{\eta}^2$ is the element-wise square of the slack variable $\boldsymbol{\eta}$, and $\boldsymbol{R}_g$ is the position vector, relative to the lunar center, that locates the surface site on the moon as specified by the latitude θ_g and longitude δ_g coordinates associated with the ground site. In body-fixed coordinates

$$\boldsymbol{R}_g = r_M \left\{ \begin{array}{c} \cos\theta_g \cos\delta_g \\ \cos\theta_g \sin\delta_g \\ \sin\theta_g \end{array} \right\} \quad [10]$$

and r_M is the mean radius of the moon. Note that $\boldsymbol{R}$ and $\boldsymbol{R}_g$ must be expressed in terms of the same frame for use in Eqn. [9]. This common vector basis is achieved by transforming $\boldsymbol{R}_g$, in the body-fixed frame, to the inertial frame using the libration angles available from the JPL DE405 ephemeris file. The path constraint, Eqn. [9], forces the coverage trajectory to remain within an instantaneous cone with a vertex at the terminal point of the vector $\boldsymbol{R}_g$, i.e., at the lunar surface site, and the cone axis parallel to $\boldsymbol{R}_g$.

Using collocation, a solution is determined by discretizing the continuous solution $\boldsymbol{X}(t)$ into many points, or nodes. The collocation algorithm is based on the 12th-order scheme as developed by Herman.[20] The control, $\boldsymbol{u}(t)$ is assumed to be piecewise linear, as specified by the node control points which are allowed to vary freely. The points are subsequently interpolated with a seventh-degree polynomial and the polynomial is forced to satisfy Eqns. [3] and [9]. The number of nodes and the spacing in time, i.e. the mesh, is adjusted to meet a specified integration tolerance. The mesh refinement procedure in this analysis is an adaption of de Boor.[21] The complete collocation and mesh refinement algorithm is presented in Ozimek et al.,[16] where it is tested against standard explicit propagators in MATLAB®.

Each segment along the path in each phase is structured consistent with Fig. 4, where $T_{b,j}$ is the burn duration for the j^{th} thrust arc, comprised of $n_{b,j}$ nodes. Similarly, $T_{c,j}$ is the coast duration for the j^{th} coast arc, comprised of $n_{c,j}$ nodes. The number of thrust arcs is determined by the user, and a coast arc is always inserted between two thrust arcs. The initial guess for phase #2 is the trajectory represented in Fig. 2. For phase #1, the equations are explicitly integrated, originating from the ISS using a velocity pointing law. When the geometry between the sun-spacecraft, Earth-spacecraft, and Earth-sun vectors indicates eclipsing conditions, the engine is turned off, i.e. $\boldsymbol{f}_T = 0$ because power is unavailable from the solar arrays. Additionally, the spacecraft experiences no SRP during the eclipse, and therefore $S_0 = 0$ in Eqn. [7]. The initial spiral-out terminates when the trajectory is observed to escape from the vicinity of the Earth. The remaining portion of the phase #1 trajectory is assumed to follow a thrust-coast-thrust pattern, and an initial guess is determined with explicit integration by varying the time associated with each arc until the final state approximately matches the initial state that defines the start of phase #2. Only this portion of phase #1 (the transfer from the initial spiral-out to the coverage orbit) is adjusted in the collocation scheme (i.e., the initial spiral-out from the ISS is fixed). Similarly, an initial guess for phase #3 is computed by assuming frozen orbit conditions and explicitly integrating backwards using an anti-velocity pointing law.

Once an initial guess is available, the constraints and variables are constructed as described in Grebow et al.[8] For the higher-fidelity model, the problem parameters for the thrust and coast arcs are initial mass, initial time, and arc duration. As in the previous study, the problem parameters are assumed independent for each collocation segment and constraints are added to enforce equality in the parameters across the arc. (This assumption to maintain independent constraints aids in the numerical efficiency for large-dimensioned, sparse problems.) Additionally, there are constraints to ensure that arc duration is always positive and that initial mass and initial time for each arc is consistent with $T_{b,j}$ and $T_{c,j}$. The boundary conditions fix an initial state, control, time, and mass at the initiation of the variable portion of phase #1. Boundary conditions are also applied to ensure state, control, time, and mass continuity between the phases. Finally, a boundary condition forces the final state along the phase #3 trajectory arc to correspond to a semi-major axis, inclination, eccentricity, and argument of periapsis consistent with conditions provided by Ely[5] for the final lunar frozen orbit. Constraints also force the insertion point into the lunar orbit to occur at apoapsis of the frozen orbit and in the x-z plane associated with the Earth-moon pulsating, rotating frame. A feasible solution is computed with SNOPT. Consistent with Grebow et al.,[8] the feasible solution is then employed as an initial guess for the direct maximization of the total time in phase #2. All constraint tolerances are set to the SNOPT defaults (10^{-6}), and the mesh refinement tolerances are input as 10^{-8}.

NUMERICAL RESULTS

The solution procedure is successfully used to compute feasible and optimal solutions to the three-phase pole-sitter scenario in a higher-fidelity model. The constants for all relevant parameters are listed in Table 1. The Julian date at epoch corresponds to an actual International Space Station (ISS) ephemeris state vector on July 17, 2009 at 16:00:00 Universal Time (UTC). The insertion state for the trajectory at the end of phase #3 is achieved by targeting the semi-major axis a_f, eccentricity e_f, inclination i_f, and argument of periapsis ω_f corresponding to a stable lunar frozen orbit.[5] Given the engine efficiency assumed in Table 1, an engine power P of 2.3 kW, corresponding to the thrust T and I_{sp} is presented. Also included in Table 1 are the scaling parameters for both forms of the equations of motion, Eqn. [1] and Eqn. [3] (where $m_0 = 500$ kg is used to nondimensionalize the spacecraft mass and thrust magnitude), and all constants necessary to define oblateness and SRP models. Finally, in all remaining figures, blue arcs refer to coasting periods, red arcs represent thrusting periods, and green arcs identify the lunar frozen orbit, the path subsequent to the completion of phase #3. Black dots denote an engine switch or a phase interface to be discussed.

To illustrate phase #1, a complete Earth-centered, EMEJ2000 (ECI) view of both the feasible and optimal solutions appears in Fig. 5. Note that the black point labeled '1' near the center of the figure corresponds to the interface between the fixed portion of phase #1 that remains constant in both the feasible and optimal solution, and the portion that enters as part of the collocation and optimizing procedure, combined with the other phases. An initial observation of the fixed transfer portion that precedes the '1' label is that there are notable regions of coasting during the long-duration Earth spiral-out. These engine-off durations result from shadowing, and ultimately cause 21.86 days of additional coasting, which is a 9.09% increase in total transfer time for the phase #1 feasible solution and a 9.46% increase for the optimal solution. Compared to the previous analysis within the context of the RTBP, the feasible transfer in the full model requres an extension of

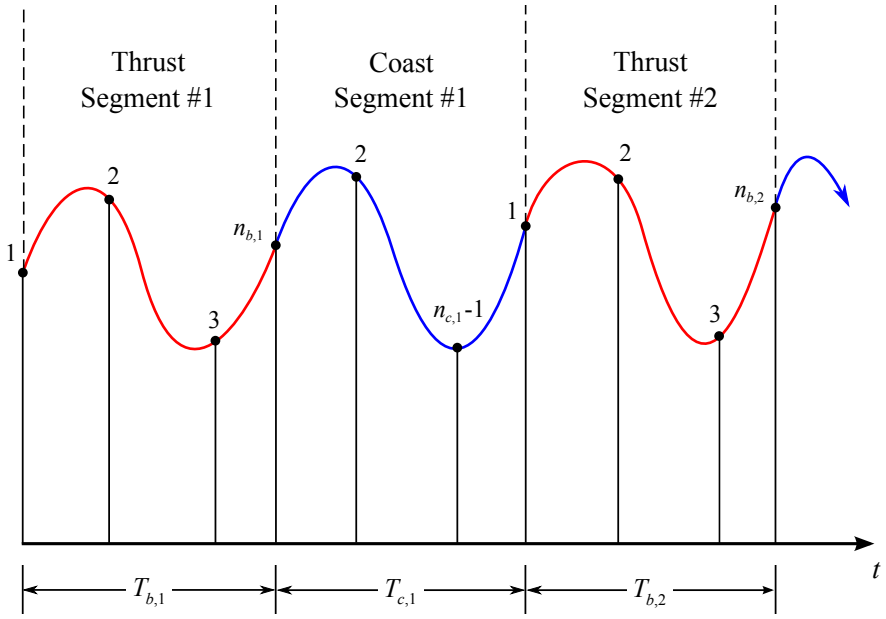

Fig. 4 Thrust-Coast Problem Structure.

17.35 days, or an additional 7.08%, and the optimal trajectory requires an interval that is longer by 16.59 days, or an additional 7.02%. More extensive durations of shadowing are avoided because of the relatively high 51.6° inclination of the ISS departure orbit, as opposed to a departure within the ecliptic plane. In Fig. 5, it is also noted that beyond the point labeled '1,' the optimal solution retains a much larger out-of-plane thrusting arc that reduces the time and the fuel consumed to expend both later in phase #2. This remarkable behavior highlights the importance of optimizing the time-of-flight in phase #2, subject to the design variables within the other phases. From the thrust-coast-thrust structure in phase #1 that is apparent in the feasible solution, the transfer corresponding the optimal solution also relocates the large coast arc such that it is more efficiently incorporated near the moon for the start of phase #2. For further data regarding phase #1, see Table 2.

Since the remaining phases are difficult to interpret as viewed in Fig. 5, phase #2 and phase #3 appear in the International Astronomical Union (IAU) frame (Fig. 6), and the moon-centered, rotating, pulsating frame. (See Fig. 7.) Note that the IAU frame is a moon-centered inertial frame with a z-axis directed towards the lunar north pole. For reference, the points along the trajectory as it enters phase #2 and phase #3 noted in both the feasible and optimal solutions, are identified with corresponding '2' and '3' labels in Fig. 7. The IAU plots in Fig. 6 best reflect the continuous surveillance of both solutions in inertial space, as the coverage orbits maintain a crown-like shape that constantly hovers within direct line-of-sight of the Shackleton crater. (Ely describes the IAU frame as a natural frame for lunar south pole trajectory design.[5]) The rotating, pulsating plots in Fig. 7 are useful for examining the similarity to the initial guess from the RTBP. (Compare with Fig. 2). In both of the views in Fig. 6 and Fig. 7, it is apparent that the optimizing objective to maximize the time-of-flight during phase #2 is partly achieved by determining an orbit configuration that extends the allowable coast arc durations. As a result, the optimal orbit utilizes coast arcs that 'touch' the boundary of the prescribed altitude upper limit, whereas the feasible solution does not. Surprisingly, the optimal coverage orbit reaches altitudes as low as 7,941 km, as the final revolutions of the trajectory appears to pass closely by the moon into the L_1 region before dropping into the lunar stable orbit. Even though the total fuel mass is fixed at 450 kg, the optimal orbit manages to utilize an additional 8.6 kg of fuel (from phases #1 and #3) due to the multi-phase direct transcription formulation. In the case of the optimal solution, only 0.89 kg are necessary to transfer into the lunar frozen orbit. Note that the lunar frozen orbit is propagated for several months to demonstrate its stable behavior without the use of any fuel.

In both the feasible and the optimal trajectories, the minimum elevation angle is equal to the minimum allowable value of $\phi_{lb} = 6°$. This result is 7° smaller than the previous study by Grebow et al.[8] due to the inclusion of lunar librations and the requirement to maintain line-of-sight with the ephemeris coordinates of the Shackleton site, rather than a static south pole reference. A time history of elevation angle performance is detailed in Fig. 8. Here, some additional insight is also available between the two solutions. In the feasible solution, coast arcs are short or non-existent during the beginning segments of the trajectory. The coast arcs gradually elongate as the trajectory evolves. The minimum elevation angle also *increases* as time progresses. This initially unforeseen natural behavior evolves from the simple

Table 1 Problem Constants.

Parameter	Value	Units
Julian date at epoch	2455030.16666667	days
X_0	$-217,157.872523697$	km
Y_0	$-265,663.694939137$	km
Z_0	$-143,797.489787933$	km
$\dot{X}_0$	7.14747905069707	km/s
$\dot{Y}_0$	-0.072004027654518	km/s
$\dot{Z}_0$	-4.64811621321917	km/s
θ_g	-89.9	$^\circ$
δ_g	0	$^\circ$
a_f	6,541.4	km
e_f	0.6	$^\circ$
i_f	56.2	$^\circ$
ω_f	-90	$^\circ$
a_{ub}	100,000	km
ϕ_{lb}	6	$^\circ$
l^*	384,431.4584485	km
t^*	375,236.314564115	s
μ_M	4,902.799140594719	km^3/s^2
μ_E	398,600.4480734463	km^3/s^2
μ_S	132,712,439,935.4841	km^3/s^2
r_m	1,738	km
r_e	6,378.14	km
J_2	0.0010827	
m_0	500	kg
m_f	50	kg
T	150	mN
I_{sp}	1,650	s
P	2.3	W
Engine efficiency	0.527640407608696	
g_0	9.80665	m/s^2
k	1.4	
S_0	1,358.098	W/m^2
A	3.14159265358979	m^2
c	299,792.458	km/s
r_0	149,597,927	km

initial guess strategy, and may correspond to another desirable performance characteristic for a pole-sitter that is available at the expense of additional fuel mass. In contrast, the optimal solution employs more coast arcs at the beginning of the trajectory, and arcs along the trajectory continue to occasionally extend to the 6° minimum elevation boundary. Another noted feature of the collocation process is that a thrust or a coast arc can be automatically eliminated by shrinking its time to zero if it is unnecessary for the final solution.

In total, optimization results in 451.26 days of coverage time, an increase of 64.58 days, or 16.70% with only the 8.6 kg of additional fuel used in phase #2. (See Table 2.) As previously noted,[8] the large increase in time-of-flight with only a small amount of additional fuel indicates that the optimizer locates an entirely new dynamical solution primarily through the use of coast arc placement. This optimal solution in the full model is still 102.92 days shorter than the result in the RTBP model by Grebow,[8] but both solutions are *locally* optimal and may not be indicative of a true globally optimal comparison. Some of the time difference may also be attributable to the behavior in the out-of-plane departure orbit. Compared to the study in the RTBP model, the higher-fidelity departure spiral is a more complex transfer trajectory with many higher-fidelity perturbations, and ultimately requires more fuel mass.

CONCLUSION

Building on a previous study in a simplified dynamical model, an optimal low-thrust pole-sitter mission trajectory is computed in a higher-fidelity model. This mission scenario could be useful for continuous lunar south pole relay communications using only one spacecraft, and possibly other lunar applications. The trajectory is also computed such that it can serve as part of a larger, long-duration re-

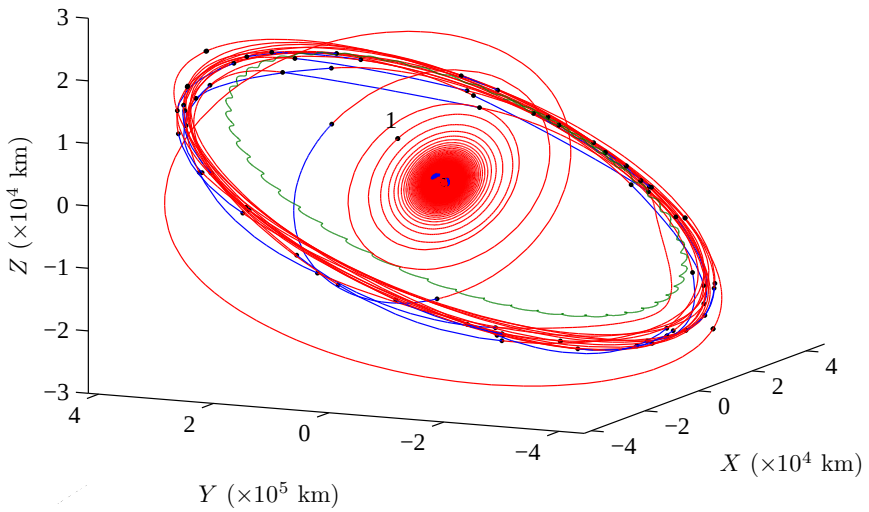

a) Feasible

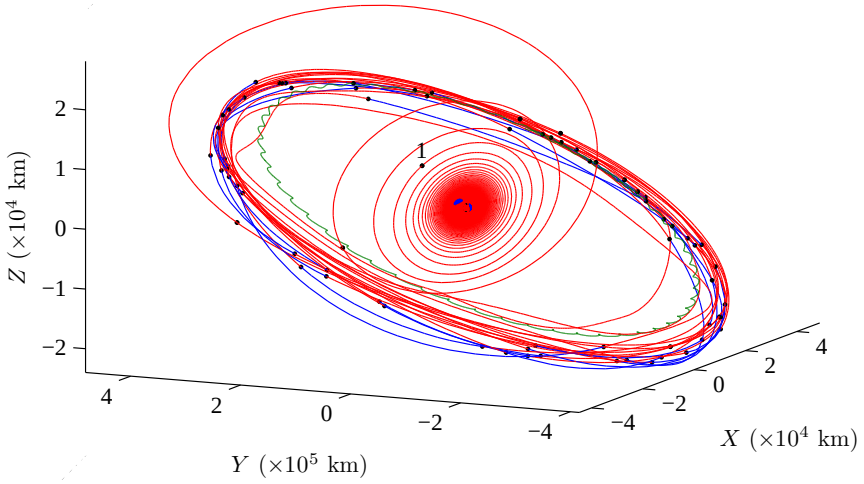

b) Optimal

Fig. 5 Three-Phase Solution in the Earth-Centered EMEJ2000 Frame.

Table 2 Performance Comparison of Feasible and Optimal Three-Phase Solutions.

		RTBP[8]		FULL	
		Feasible	Optimal	Feasible	Optimal
PHASE #1	Fuel Mass Consumed (kg)	184.10	175.55	188.61	185.04
	Total Time (days)	244.97	236.30	262.32	252.89
PHASE #2	Fuel Mass Consumed (kg)	264.19	273.09	255.01	263.61
	Total Time (days)	447.04	554.18	386.68	451.26
	Min. Altitude (km)	32,400	24,750	29,916	7,941
	Max. Altitude (km)	80,000	100,000	97,364	100,000
	Min. Elevation Angle (°)	13.0	13.0	6.0	6.0
	Max. Elevation Angle (°)	79.5	60.5	67.5	70.0
PHASE #3	Fuel Mass Consumed (kg)	1.76	1.41	1.90	0.89
	Total Time (days)	2.36	2.37	2.37	1.11

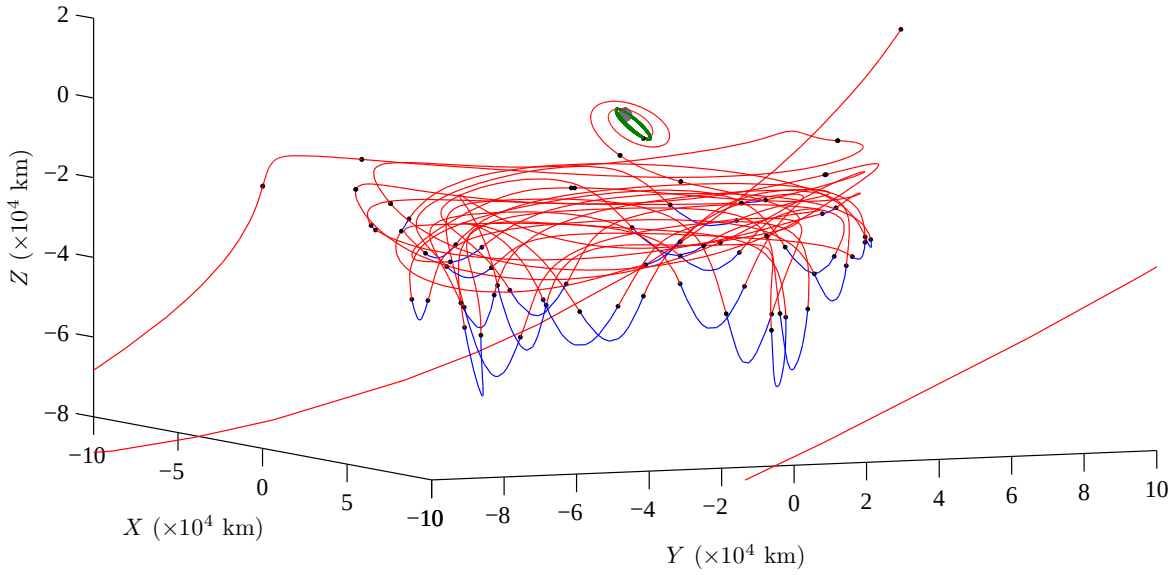

a) Feasible

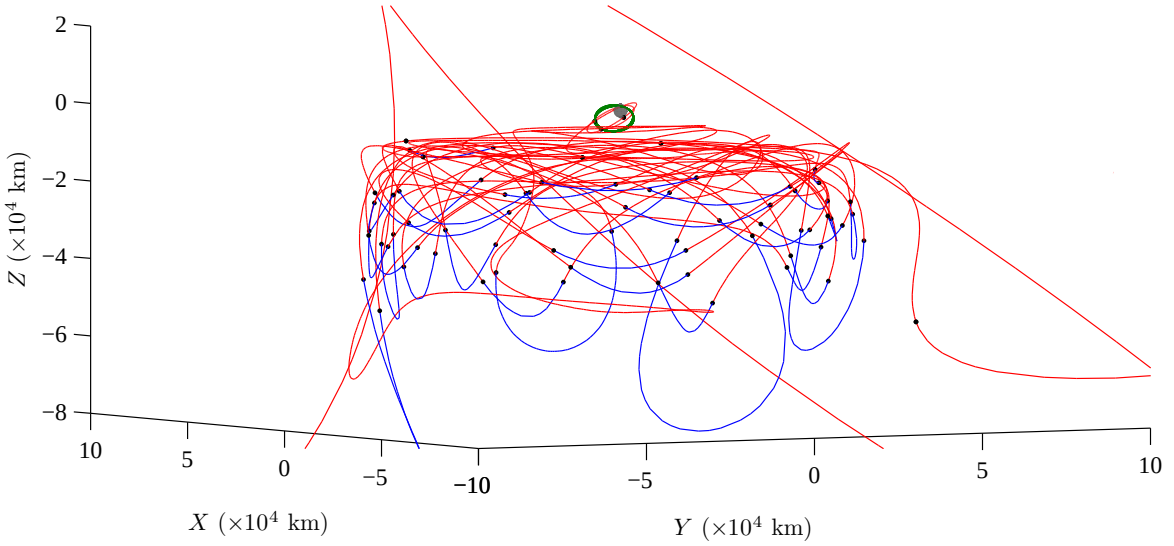

b) Optimal

Fig. 6 Coverage Orbit (Phase #2) and End-of-Life (Phase #3) in the IAU Frame.

lay using stable lunar frozen orbits. The computation of this complex, numerically sensitive, multi-phase trajectory is handled in sequence by computing each phase individually. The coverage orbit is prioritized, and the underlying dynamical properties, apparent in the RTBP, yield insight to produce an initial orbit. The orbit is then transitioned and combined with the other phases of interest in a full dynamical model, and a newly implemented mesh refining procedure ensures that the resulting discrete solution accurately reflects the continuous dynamics. Since a low-thrust pole-sitter will ultimately exhaust the available fuel while offsetting gravity, a direct transcription optimizing procedure maximizes the time prior to this event, ultimately yielding an increase of 16.7% in time-of-flight. This time increase is dependent on the fuel mass available, but still demonstrates the usefulness of an optimizing process. Other performance objectives besides time could clearly be considered and implemented, especially as solar sail technology evolves. Furthermore, additional perturbing effects can be added to the model without significantly altering the general solution method. The implementation of the current design under the influence of many higher-fidelity dynamical effects verifies that the low-thrust pole-sitter trajectory concept remains a viable option for temporary lunar

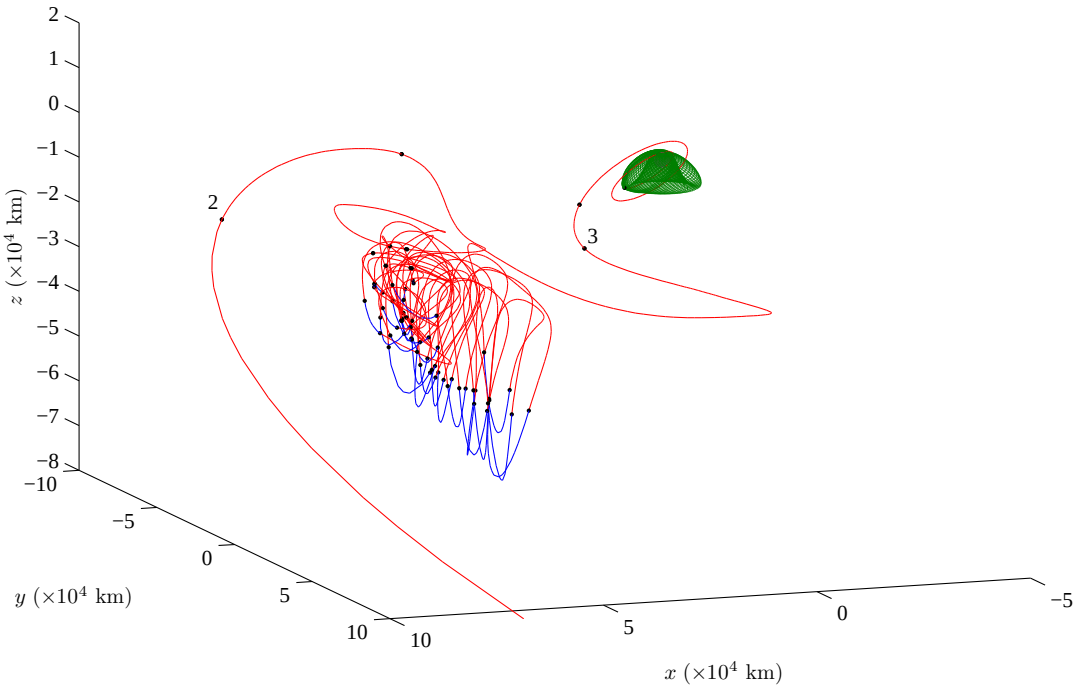

a) Feasible

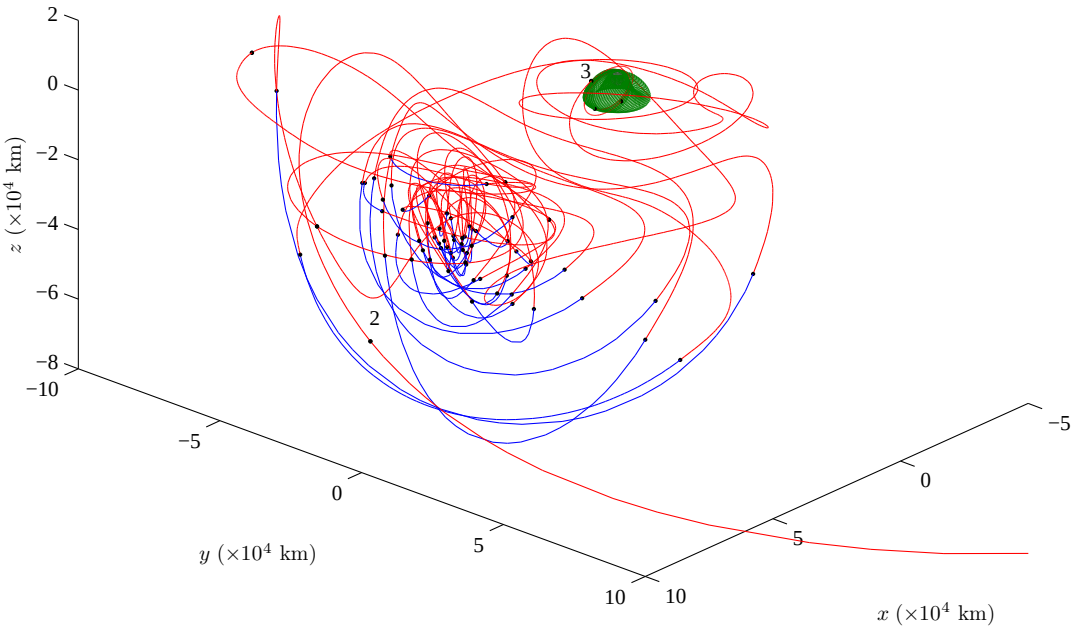

b) Optimal

Fig. 7 Coverage Orbit (Phase #2) and End-of-Life (Phase #3) in the Moon-Centered, Pulsating, Rotating Frame.

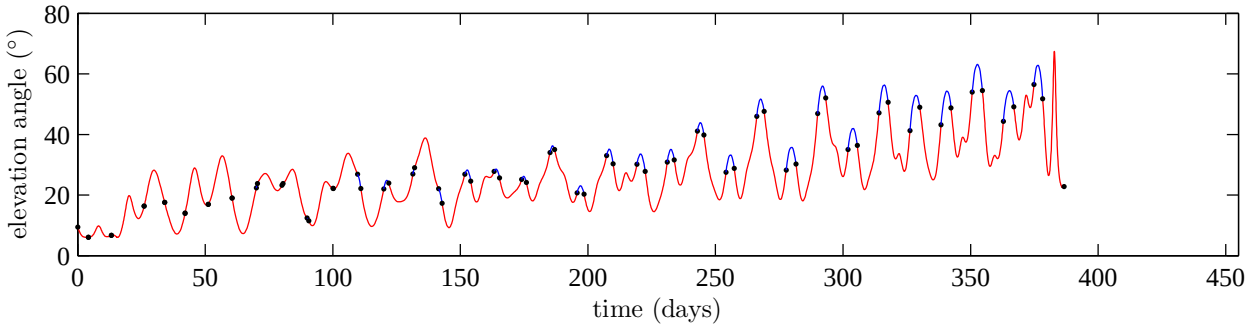

a) Feasible

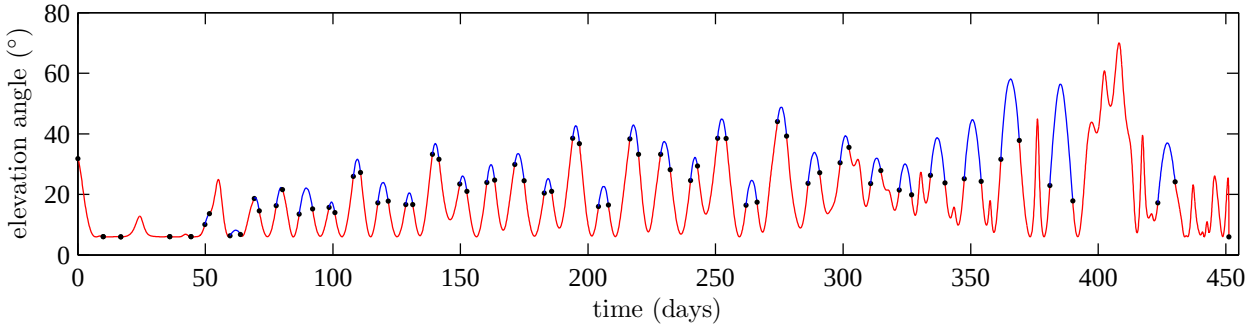

b) Optimal

Fig. 8 Elevation Angle Time History.

south pole coverage.

ACKNOWLEDGEMENTS

This work was supported by the NASA Graduate Student Researchers Program (GSRP) fellowship under NASA Grant No. NNX07A017H and the Purdue University Graduate Assistance in Areas of National Need (GAANN) fellowship. The authors also thank Wayne Schlei for importing trajectories and useful animations into Purdue University's Rune and Barbara Eliason Advanced Visualization Laboratory.

REFERENCES

[1]"SELENE: SELenological ENgineering Explorer "KAGUYA"," [Online Publication], http://www.jaxa.jp/pr/brochure/pdf/04/sat16.pdf [retrieved 30 September 2009].

[2]"Lunar Reconnaissance Orbiter (LRO): Leading NASA's Way Back to the Moon, Lunar Crater Observation and Sensing Satellite (LCROSS): NASA's Mission to Search for Water on the Moon," [Online Publication], http://www.nasa.gov/pdf/360020main_LRO_LCROSS_presskit2.pdf [retrieved 15 September 2009].

[3]"Chandrayaan: Lunar Mission by Indian Space Research Organization," [Online Publication], http://www.chandrayaan-i.com/index.php [retrieved 30 September 2009].

[4]C. Pieters, J. Goswami, R. Clark et al., "Character and Spatial Distribution of OH/H_2O on the Surface of the Moon," *Science Magazine*, [Online Publication], http://www.sciencemag.org/cgi/rapidpdf/1178658v1.pdf [retrieved 30 September 2009].

[5]Ely, T., "Stable Constellations of Frozen Elliptical Inclined Orbits," *Journal of the Astronautical Sciences*, Vol. 53, No. 3, 2005, pp. 301-316.

[6]Grebow, D., Ozimek, M., Howell, K., and Folta, D., "Multibody Orbit Architectures for Lunar South Pole Coverage," *Journal of Spacecraft and Rockets*, Vol. 45, No. 2, 2008, pp. 344-358.

[7]Ozimek, M., Grebow, D., and Howell, K., "Solar Sails and Lunar South Pole Coverage," *Journal of Guidance, Control, and Dynamics*, Vol. 32, No. 6, November-December 2009. (to appear)

[8]Grebow, D., Ozimek, M., Howell, K., "Design of Optimal Low-Thrust Lunar Pole-Sitter Missions," Paper No. AAS 09-148, *19th AAS/AIAA Space Flight Mechanics Meeting*, Savannah, Georgia, February 8-12, 2009.

[9]Bell, J., "The Impact of Solar Radiation Pressure on Sun-Earth L1 Libration Point Orbits," M.S. Thesis, School of Aeronautics and Astronautics, Purdue University, West Lafayette, Indiana, July 1991.

[10]McInnes, C., "Solar Sail Trajectories at the Lunar L_2 Lagrange Point," *Journal of Spacecraft and Rockets*, Vol. 30, No. 6, 1993, pp. 344-358.

[11]Kluever, K. and Oleson, S., "Direct Approach for Computing Near-Optimal Low-Thrust Earth-Orbit Transfers," *Journal of Spacecraft and Rockets*, Vol. 35, No. 4, July-August 1998, 509-515.

[12]Kechichian, J., "Orbit Raising with Low-Thrust Tangential Acceleration in Presence of Earth Shadow," *Journal of Spacecraft and Rockets*, Vol. 35, No. 4, July-August 1998, pp. 516-525.

[13]Flandro, G., "Asymptotic Solution for Solar Electric Low Thrust Orbit Raising with Eclipse Penalty," Paper No. 74-802, *AIAA Mechanics and Control of Flight Conference*, Anaheim, California, August 5-9, 1974.

[14]McInnes, C., "Low-Thrust Orbit Raising with Coupled Plane Change and J_2 Precession," *Journal of Guidance, Control, and Dynamics*, Vol. 20, No. 3, pp. 607-609.

[15]Hargraves, C., and Paris, S., "Direct Trajectory Optimization Using Nonlinear Programming and Collocation," *Journal of Guidance, Control, and Dynamics*, Vol. 10, No. 4, 1987, pp. 338-342.

[16]Ozimek, M., Grebow, D., and Howell, K., "A Collocation Approach for Computing Solar Sail Lunar Pole-Sitter Orbits," Paper No. AAS 09-

378, *AIAA/AAS Astrodynamics Specialists Conference*, Pittsburgh, Pennsylvania, August 2009.

[17]Betts, J. and Huffman, P., "Application of Sparse Nonlinear Programming to Trajectory Optimization," *Journal of Guidance, Control and Dynamics*, Vol. 15, No. 1, 1990, pp. 198-206.

[18]Gill, P., Murray, W., and Saunders, M., "SNOPT: An SQP Algorithm for Large-Scale Constrained Optimization," *SIAM Review*, Vol. 47, No. 1, pp. 99-131.

[19]Farquhar, R., "The Control and Use of Libration-Point Satellites," NASA TR R-346, September 1970.

[20]Herman, A., "Improved Collocation Methods with Applications to Direct Trajectory Optimization," Ph.D. Dissertation, Department of Aerospace Engineering, University of Illinois at Urbana-Champaign, Urbana, Illinois, September 1995.

[21]de Boor, C., "Good Approximation by Splines with Variable Knots. II," *Conference on the Numerical Solution of Differential Equations, Lecture Notes in Mathematics*, Vol. 363, Springer, New York, 1973.